ISSN 1470-5559

Color Filter Arrays: A Design Methodology

Yan Li, Pengwei Hao, and Zhouchen Lin

Queen Mary
University of London
Department of Computer Science

RR-08-03 May 2008

Color Filter Arrays: A Design Methodology

Yan Li[*], Pengwei Hao[†], and Zhouchen Lin[‡]

Abstract

In the companion report [14], we have shown that a full color image sampled with a rectangular color filter array (CFA) is equivalent to the frequency domain multiplexing of multiplex components: a luminance component (luma) at the baseband and several chrominance components (chromas) at high frequency bands. A matrix, called the frequency structure of a CFA, is defined to represent this modulation, with which we can easily analyze the characteristics of CFAs. The frequency structure can be computed by applying the symbolic discrete Fourier transform (DFT) to the CFA pattern. In this paper, we present a CFA design methodology in the frequency domain. In this methodology, a good frequency structure of the CFA is first selected, mainly according to the following criteria: (i). the number of nonzero chromas should be as small as possible; (ii). the distance between nonzero multiplex components should be as large as possible; and (iii). dependent (e.g., identical, negative, or conjugate) chromas should be as many as possible; and then the optimal primary CFA patterns are computed by minimizing the norm of the demosaicking matrix under constraints that: (i). the primary CFA patterns are all real and nonnegative; and (ii). their sum is an all-one matrix. The constraints can be determined by applying the inverse symbolic DFT to the specified frequency structure. Finally, the desired CFA pattern is the symbolic sum of the optimal primary CFA patterns. Using our methodology, a series of new CFA patterns are found which outperform the currently commercialized and published ones. Experiments demonstrate the effectiveness of our CFA design methodology and the superiority of our new CFA patterns.

Keywords: color filter array (CFA), discrete Fourier transform (DFT), sampling, multiplexing, demosaicking

[*]Y. Li is with the State Key Laboratory of Machine Perception, Peking University, Beijing 100871, China (e-mail: yanli8083@gmail.com).

[†]P. Hao is with the Department of Computer Science, Queen Mary, University of London, London E1 4NS, U.K.,(e-mail: phao@dcs.qmul.ac.uk).

[‡]Z. Lin is with Microsoft Research Asia, 5th Floor, Sigma Building, Zhichun Road 49#, Haidian District, Beijing 100080, China (e-mail: zhoulin@microsoft.com).

1 Introduction

To reduce cost, size, and complexity, many digital cameras use only one single-chip sensor covered with a *Color Filter Array* (CFA) [1, 19] (Fig. 1). Therefore, at each pixel only one color can pass the filter of the CFA and be sensed. The missing colors have to be estimated by methods referred to as demosaicking [8]. Hundreds of demosaicking algorithms have been proposed, which mainly target the Bayer CFA (Fig. 1(a)) and have become more and more complicated. However, there is another crucial factor that has great impact on the quality of the demosaicked images: the CFA design, i.e., the choice of CFA patterns [15]. A CFA pattern is one period of the CFA (The readers are encouraged to refer to the companion report [14] for the definitions of terminologies).

The most commonly used CFA pattern is the Bayer pattern (Fig. 1(a)) [3], whose sampling rates for green, red, and blue (G, R, and B) are 1/2, 1/4, and 1/4, respectively. The Bayer pattern was designed based on two facts of the human visual system (HVS): relatively greater ability to discern luminance detail, and the closeness of green wavelengths to the peak of the human luminance frequency response [3], [7]. As an alternative, Bayer further adjusted the sampling rates for R, G, and B (to 1/2, 3/8, 1/8, respectively) to the acuity of the HVS [3], since human vision has the lowest sensitivity to blue detail.

Based on the Bayer pattern, some other patterns have been proposed for better imaging. Since the green channel has a closer relationship to the luminance and hence has more energy in a natural image, green sensors saturate faster than those of red and blue. So the Bayer CFA, half of which is for green, would perform badly when overexposure happens. This problem was tackled in [20] by introducing the luminance channel (W), which would saturate first while R, G, and B are still accurate when overexposed (Fig. 1(b)). However, the CFA in [20] would suffer a great loss of spatial resolution because 50% of the sensors are for luminance. An improved pattern, whose sampling rates for W, R, G, and B are equal (all 1/4), was proposed in [6] (Fig. 1(c)). To deal with low light conditions, a CFA pattern using subtractive colors, such as cyan, magenta, yellow (C, M, Y) and green, was proposed in [9] (Fig. 1(d)). By introducing a light blue color emerald (E), Sony announced a new CFA pattern RGBE (Fig. 1(e)), claiming that the pattern is closer to the natural sight perception of the human eye and, by combining with a new processor, the color reproduction errors could be reduced by half and the reproduction of blue, green, and red colors could be particularly enhanced [18]. Quite recently, Kodak announced a few new CFA patterns (Fig. 1(f)-(g)) featuring one 'panchromatic pixel' (luminance) adjacent to every colored pixel (R, G, or B), to increase the overall sensitivity of the sensor and enable faster shutter speeds and the design of smaller pixels [13].

By investigating random sampling when undersampled, whose effect is to eliminate the aliased spectrum that occurs under regular sampling and replace it with a noise-like spectrum of lower amplitude, some random (stochastic) patterns were proposed in [22] (Fig. 1(h)). Pseudo-random (or random) CFAs were also recommended in [5, 15] for being more immune to color Moiré artifacts (Fig. 1(i)).

By analyzing the spectral properties of the HVS, a quantitative analysis was given in [16] to design CFA patterns with minimum perceptual error (Fig. 1(j)), i.e., to minimize the discrepancy between the reconstructed and the original images when using the filters simulating the HVS. The authors also investigated

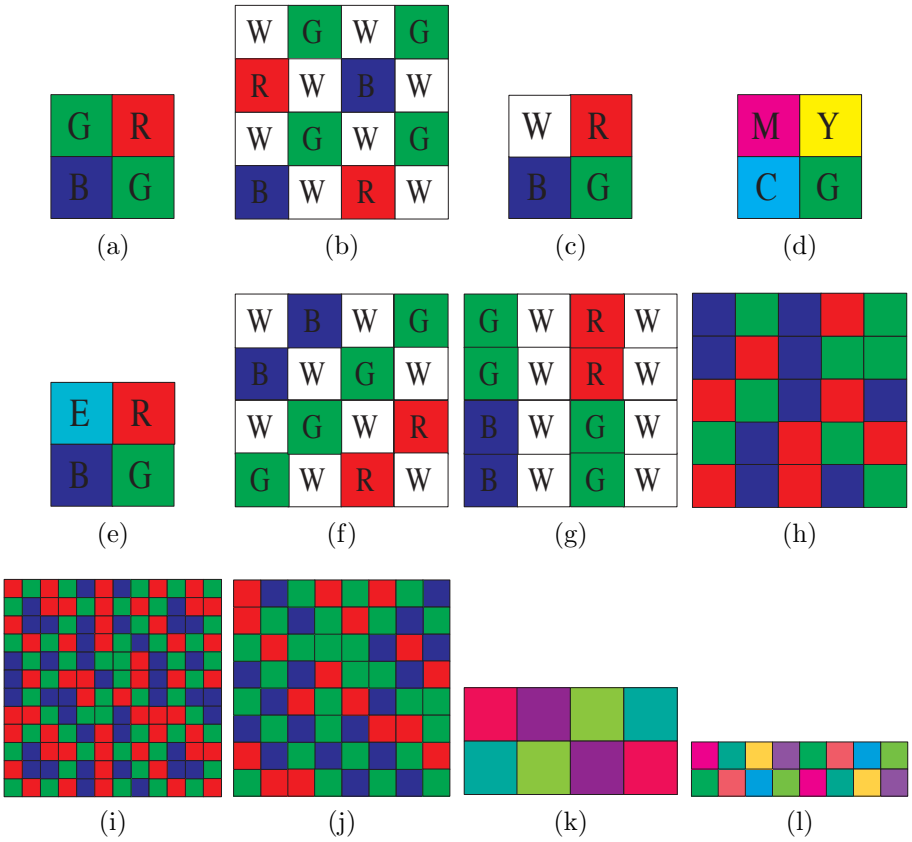

Figure 1: Some published CFA patterns. (a) Bayer [3], (b) Yamagami et al. [20], (c) Gindele & Gallagher [6], (d) Hamilton et al. [9], (e) Sony [18], (f)-(g) Kodak [13], (h) Zhu et al. [22], (i) Fillfactory [5], (j) Parmar & Reeves [16], (k)-(l) Hirakawa & Wolfe [11].

how to select spectral sensitivity functions [17], rather than just ordinary R G and B, or C M and Y transmittances, for filters in the CFA pattern. The visible spectrum was sampled every 10 nm in the range of 400-700nm and thus each spectral sensitivity function was represented by a 31-dimensional vector. Three or four different spectral sensitivity functions were obtained by minimizing the reconstruction error under different illuminants in the CIE $L^*a^*b^*$ space (a perceptually uniform color space).

Based on the spatio-spectral sampling properties of the corresponding lattices of CFA patterns, a CFA design method in the Fourier domain was proposed in [11] (Fig. 1(k)-(l)). The sensed image was represented by the sum of a baseband component (luma) and some modulated signals (chromas), and CFA design was turned into a problem of parameters selection in the Fourier domain in order to separate the modulated signals from the baseband spectrum at the best. Three new CFA patterns were proposed in the paper, which all outperform the Bayer pattern. Using their spectral representation, the authors also studied how to design CFAs for digital image display devices considering the spatial resolution and human vision [12].

In this paper, we propose a systematic CFA design methodology. Although both our methodology and that in [11] are based on analysis in the frequency domain, our framework drastically differs from that in [11] because:

1. The objective in [11] is to separate the luma and chromas as far as possible, while ours is to recover the spectra of the primary color channels (e.g., R, G, and B) of the original image as accurately as possible. So we would allow identical (or negative, or conjugate) chromas coexist in order to estimate the chromas more robustly, rather than simply minimizing the number of chromas.

2. To achieve our goal, we propose much more criteria that a good CFA should obey, rather than only making the multiplex components as far from each other as possible.

3. And we also require the norm of the demosaicking matrix (the inverse of the multiplexing matrix) to be minimized such that the errors in estimating the luma and chromas are less amplified when they are transformed back to the spectra of the primary color channels.

Moreover, our methodology is better established on a theoretical foundation. We have proposed using a matrix, called the frequency structure, as a representation of a CFA pattern [14]. It records all the multiplexing information and is visually intuitive for qualitatively analyzing the properties of the CFA pattern. While in [11], only the form of the Fourier transform of images sampled with a CFA was given, whose parameters are unknown and thus makes it difficult to analyze a CFA. In addition, with our well established theory, the formulation of finding the optimal CFA pattern given the frequency structure and the subsequent computation method are straightforward. In contrast, the method in [11] for selecting optimal parameters to satisfy some given design criteria was unclear.

This paper is organized as follows. In Section 2, we propose CFA design principles aiming at minimizing the demosaicking error, i.e., to estimate the multiplex components as accurate as possible and to minimize the error propagation when the multiplex components are transformed back to the primary color spectra. The realization of these principles via frequency structure customization and demosaicking matrix norm minimization is elaborated in Section 3 and 4, respectively. Section 5 gives a simple design example in detail, and also proposes some new CFA patterns. Experimental results and comparisons between the Bayer CFA, the three CFAs proposed in [11], and our newly proposed ones are presented in Section 6. Finally, we conclude our paper in Section 7.

2 CFA Design Principles

We believe that a good CFA should minimize the demosaicking error. In the frequency domain, a good CFA should enable good recovery of the spectra of the primary color channels of the original image. In the companion report [14], we have shown that the spectrum of a CFA-filtered image is the mixture of multiplex components centered (or modulated) at certain frequency points, where each multiplex component is further a mixture of the spectra of the primary color channels of the original image. All these can be conveniently represented by the frequency structure of the CFA. Therefore, we can estimate

each multiplex component first and then transform them back to the spectra of the primary color channels. We call this method the *universal demosaicking algorithm*. So it becomes clear that in order to minimize the demosaicking error, we should estimate the multiplex components as accurately as possible, and make the transform as stable as possible in order to less amplify the error in the multiplex components. These are the principles that guide our CFA design. In the following, we give more details.

2.1 Frequency structure of CFA

The frequency structure is a visually intuitive representation of a CFA. It is a matrix S with each entry being defined as:

$$\begin{aligned} S(k_x, k_y) = \quad & \sum_{\mathcal{C}} H_p^{(\mathcal{C})}\left(\frac{k_x}{n_x}, \frac{k_y}{n_y}\right) \cdot F^{(\mathcal{C})}(\omega_x, \omega_y), \\ & k_x = 0, 1, \cdots, n_x - 1, \\ & k_y = 0, 1, \cdots, n_y - 1. \end{aligned} \tag{1}$$

where $\mathcal{C} = R, G$, and B, (or other primary colors), $H_p^{(\mathcal{C})}$ is the DFT of the primary CFA pattern $h_p^{(\mathcal{C})}$ for the color channel $\mathcal{C}$, $F^{(\mathcal{C})}$ is the DFT of the $\mathcal{C}$ component image $f^{(\mathcal{C})}$, and (n_x, n_y) is the size of the CFA pattern h_p. Eq. (1) means that at frequencies $\left(\frac{k_x}{n_x}, \frac{k_y}{n_y}\right)$ there are spectral components $\sum_{\mathcal{C}} H_p^{(\mathcal{C})}\left(\frac{k_x}{n_x}, \frac{k_y}{n_y}\right) \cdot F^{(\mathcal{C})}(\omega_x, \omega_y)$ centering there, respectively. The spectrum of the CFA-filtered image is exactly the multiplexing of these spectral components by modulating them to their corresponding frequencies. For this reason, we call each entry of the frequency structure the *multiplex component*. We also call the multiplex component at the baseband ($S(0,0)$) the luma and the others the chromas.

Although the definition of the frequency structure looks complex, Theorem 1 of [14] shows that it can be conveniently and directly obtained by computing the symbolic DFT of the CFA pattern h_p:

$$S_{CFA} = DFT\left[h_p\right], \tag{2}$$

if $F^{(\mathcal{C})}$ in (1) is replaced with $\mathcal{C}$ symbolically.

For example, the frequency structure of the commonly used Bayer pattern (Fig. 1(a)) [3] is

$$S_{Bayer} = DFT\begin{bmatrix} G & R \\ B & G \end{bmatrix} = \begin{bmatrix} F_L & F_{C2} \\ -F_{C2} & F_{C1} \end{bmatrix}, \tag{3}$$

where

$$\begin{bmatrix} F_L \\ F_{C1} \\ F_{C2} \end{bmatrix} = T_{Bayer} \cdot \begin{bmatrix} R \\ G \\ B \end{bmatrix} \text{ with} \tag{4}$$

$$T_{Bayer} = \frac{1}{4}\begin{bmatrix} 1 & 2 & 1 \\ -1 & 2 & -1 \\ -1 & 0 & 1 \end{bmatrix}. \tag{5}$$

S_{Bayer} shows that the spectrum of any image sampled with the Bayer CFA has a luma F_L at the baseband, and three chromas F_{C1}, F_{C2}, and $-F_{C2}$ modulated

at frequencies $(1/2, 1/2)$, $(1/2, 0)$, and $(0, 1/2)$, respectively. The matrix T in (4) that relates the multiplex components and the spectra of primary colors is called the *multiplexing matrix*.

2.2 Universal demosaicking and CFA design principles

With the frequency structure S_{CFA} (2) of a CFA, demosaicking for any rectangular CFA can be easily done in the frequency domain. Namely, we first estimate the nonzero multiplex components, F_L, F_{C1}, and F_{C2}, etc., from the spectrum of the CFA-filtered image using band-pass filters, then obtain the spectra of primary color component images by inverting the linear system like (4), and finally apply IDFT to the spectra of the primary color components to recover the full color image. This is a *universal demosaicking* method, and the algorithm proposed in [4] is just this method applied to the Bayer CFA. However, its performance depends on the characteristics of the CFA. Simple as it is, we will show that with properly chosen CFA, we can still achieve superior demosaicking results.

The inversion of the linear system like (4) induces a matrix D as the inverse of the multiplexing matrix T. We shall call this matrix D the *demosaicking matrix*. For example, for the Bayer pattern, the demosaicking matrix is

$$D_{Bayer} = T_{Bayer}^{-1} = \begin{bmatrix} 1 & -1 & -2 \\ 1 & 1 & 0 \\ 1 & -1 & 2 \end{bmatrix}. \tag{6}$$

It is easy to see that for the universal demosaicking method to perform well, the CFA should enable the following procedures to work well:

1. to estimate the multiplex components accurately;
2. to estimate the spectra of primary color components from the multiplex components accurately.

To achieve the first goal, we have two principles:

(P1) The crosstalk among the multiplex components should be as little as possible.

(P2) The correlations among the multiplex components should be as high as possible.

With the first principle, band-pass filtering will result in little aliasing frequencies from other multiplex components. And by the second principle, we can robustly estimate the multiplex components by taking advantage of the correlation among them.

To achieve the second goal, we have to control the error in the estimated multiplex components such that it will be less amplified. Noticing the linear relationship between the multiplex components and the spectra of primary color components, this can be realized by minimizing the norm of the demosaicking matrix D. Hence we have the third principle:

(P3) The norm of the demosaicking matrix D should be minimized.

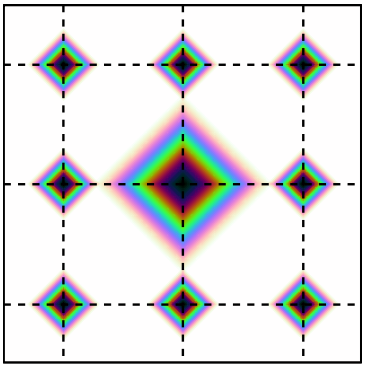

Figure 2: All possible positions of multiplex components of the sensed image by a CFA pattern of size 3×3.

Our CFA design methodology is based on these three principles. It consists of two steps: choosing an appropriate frequency structure of the CFA and choosing optimal primary CFA patterns such that the norm of D is minimized. The details are described in the following sections.

3 Choosing a CFA Frequency Structure

This section focuses on how to choose an appropriate frequency structure of the CFA in order to follow (P1) and (P2) in the previous section, i.e., specify the positions of nonzero multiplex components and designate the relationship (equal, negative, or conjugate) among the chromas.

3.1 Conditions: hard constraints

The specification of frequency structure is *not* arbitrary. First, the centers of the nonzero multiplex components can only be at the lattice $(k_x/n_x, k_y/n_y)$, $k_x = 0, 1, \cdots, n_x - 1; k_y = 0, 1, \cdots, n_y - 1$ [14]. So we can only choose among these points as the centers of nonzero multiplex components. Fig. 2 shows all possible centers of multiplex components when $n_x = n_y = 3$. Second, the luma must exist. So the frequency point $(0, 0)$ must be selected by default. Third, in order to make the designed CFA pattern real, once a frequency point $(k_x/n_x, k_y/n_y)$ in the lattice is chosen, the one $(1 - k_x/n_x, 1 - k_y/n_y)$ at its conjugate position must also be chosen. Note that the chroma at the conjugate position, which we call the *conjugate chroma*, must also be symbolically conjugate in value, i.e., the coefficients of R, G, and B channels are all conjugate to those of the chosen chroma. These two aspects of conjugate constraints can be conveniently automated by the computer. Fourth, to reconstruct three primary color components of an image, we need at least three independent multiplex components. Since the luma is already selected, two *independent* chromas must be selected. Here, that two chromas $S(p, q)$ and $S(r, s)$ are independent means that there does not exist a scalar (real or complex) c such that $S(p, q) = c \cdot S(r, s)$. If two independent chromas are chosen, the multiplexing matrix T will be of rank 3 so that the spectra of three primary colors can be determined. This

independence can also be automatically checked by the computer via symbolic computation.

Assisted by the computer, we can click on the frequency lattice to choose nonzero multiplex components. However, in order to design a good frequency structure, we have to follow some guidelines.

3.2 Guidelines: soft constraints

To apply (P1), we may first

(G1) choose as few nonzero chromas as possible; and

(G2) maximize the distance among the nonzero multiplex components.

Moreover, due to the fact that the spectra of multiplex components have long tails along the horizontal and the vertical axes and the energy of luma is much higher than those of chromas [14], which implies that the aliasing along the axes are the most severe, we may further *wish* that

(G3) the distance between luma and chromas should be large enough (e.g., no less than 0.5); and

(G4) the chromas should not be centered on the horizontal or vertical axes of the luma.

We can only wish (G3) and (G4) because they may not always be satisfied if the size of the CFA pattern is too small, due to the hard constraints in Section 3.1. For example, for CFA patterns of size 3×3 (Fig. 3(b)), (G3) cannot be satisfied, and for CFA patterns of size 2×2 (Fig. 3(a)), (G4) cannot be satisfied.

To apply (P2), we may

(G5) choose redundant nonzero chromas and make them dependent.

With redundant chromas, we can estimate each chroma more robustly by cross-checking with its redundant copies. In our current system, for simplicity we only require that a chroma is equal to another one, rather than specifying a scalar between them. This is because being equal is the least likely to amplify the error in the estimation. From the conjugate constraints in Section 3.1, once the relationship between two chromas is specified, the relationship between their conjugate chromas will be automatically determined by the computer. Note that (G5) is in conflict with (G1). Therefore, we have to make a tradeoff between (G1) and (G5).

One should be reminded that our guidelines could not result in a unique frequency structure. We could not foresee which frequency structure is optimal if we make a tradeoff among the guidelines. We have to test the obtained CFA patterns with differently specified frequency structures using benchmark images to find the best one. Nonetheless, using our guidelines one can easily rule out a vast majority of bad frequency structures: s/he only has to test a limited number of designs, which are *possibly* the optimal. This already saves a lot of effort in CFA design.

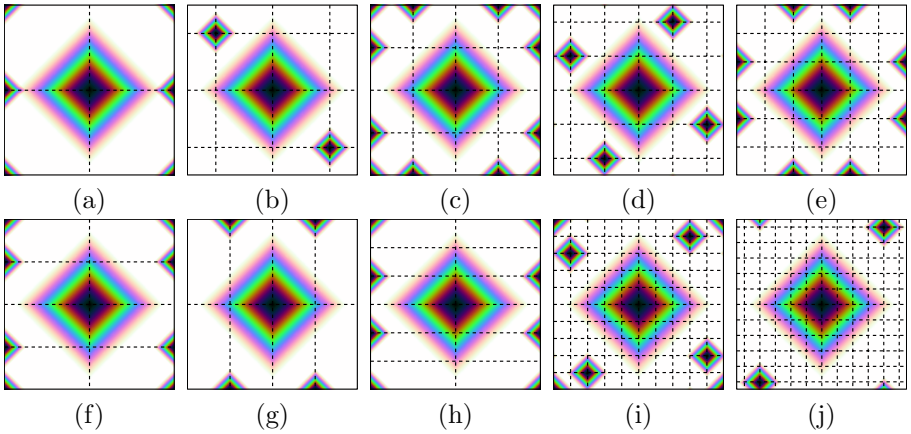

Figure 3: Some examples of frequency structures generated with CFA patterns of size (a) 2×2, (b) 3×3, (c) 4×4, (d) 5×5, (e) 6×6, (f) 4×2, (g) 2×4, (h) 6×2, (i) 10×10, (j) 11×11.

3.3 Examples of specifying the frequency structure

We show some examples of frequency structures with various sizes of CFA patterns in Fig. 3, whose corresponding frequency structures are shown in Table 1. By convention we put the baseband at the center, but all the DFT spectra are periodic in both horizontal and vertical directions, so in our frequency structure representation of CFAs, we take the frequency origin $(0, 0)$ as at the top-left corner of the matrix.

Note that the frequency structures in Figs. 3(b), (g), and (j) only have two conjugate chromas. According to the last hard constraint in Section 3.1, they must be independent. This is possible when their coefficients of R, G, and B channels do not reduce to real or imaginary numbers simultaneously. For example, the chromas $((2R - G - B) + i\sqrt{3}(G - B))/6$ and $((2R - G - B) - i\sqrt{3}(G - B))/6$ of the Diagonal stripe CFA [14] are independent. And one can also see that some frequency structures (Figs.3(c), (i)) have more than two nonzero chromas. This is because of guideline (G5).

4 Choosing Optimal Primary CFA Patterns

Once the form of the frequency structure, i.e., the size of the CFA pattern, the modulation frequencies of nonzero multiplex components, and the relationship among the chromas are chosen, the optimal primary CFA patterns can be determined by applying (P3).

As we have chosen the luma F_L and independent chromas, e.g., F_{C1} and F_{C2}, and have specified the relationship among them, the entries in the frequency structure becomes:

$$\begin{aligned} S(0,0) &= F_L, \text{ and} \\ S(k_x, k_y) &\in \{0, F_{C1}, F_{C2}, F_{C1}^*, F_{C2}^*\}, \quad (k_x, k_y) \neq (0,0), \end{aligned}$$

in which * means symbolic conjugate. The multiplex components are related to

Table 1: Frequency structures of the CFA patterns shown in Fig. 3.

$$\begin{bmatrix} F_L & F_{C1} \\ 0 & F_{C2} \end{bmatrix}$$
(a)

$$\begin{bmatrix} F_L & 0 & 0 \\ 0 & F_{C1} & 0 \\ 0 & 0 & F^*_{C1} \end{bmatrix}$$
(b)

$$\begin{bmatrix} F_L & 0 & 0 & 0 \\ 0 & 0 & F_{C2} & 0 \\ 0 & F_{C3} & F_{C1} & F^*_{C3} \\ 0 & 0 & F^*_{C2} & 0 \end{bmatrix}$$
(c)

$$\begin{bmatrix} F_L & 0 & 0 & 0 & 0 \\ 0 & 0 & F_{C1} & 0 & 0 \\ 0 & 0 & 0 & 0 & F_{C2} \\ 0 & F^*_{C2} & 0 & 0 & 0 \\ 0 & 0 & 0 & F^*_{C1} & 0 \end{bmatrix}$$
(d)

$$\begin{bmatrix} F_L & 0 & 0 & 0 & 0 & 0 \\ 0 & 0 & 0 & F_{C1} & 0 & 0 \\ 0 & 0 & 0 & 0 & 0 & 0 \\ 0 & F_{C2} & 0 & 0 & 0 & F^*_{C2} \\ 0 & 0 & 0 & 0 & 0 & 0 \\ 0 & 0 & 0 & F^*_{C1} & 0 & 0 \end{bmatrix}$$
(e)

$$\begin{bmatrix} F_L & 0 \\ 0 & F_{C2} \\ 0 & F_{C1} \\ 0 & F^*_{C2} \end{bmatrix}$$
(f)

$$\begin{bmatrix} F_L & 0 & 0 & 0 \\ 0 & F_{C1} & 0 & F^*_{C1} \end{bmatrix}$$
(g)

$$\begin{bmatrix} F_L & 0 \\ 0 & F_{C2} \\ 0 & 0 \\ 0 & F_{C1} \\ 0 & 0 \\ 0 & F^*_{C2} \end{bmatrix}$$
(h)

$$\begin{bmatrix} F_L & 0 & 0 & 0 & 0 & 0 & 0 & 0 & 0 & 0 \\ 0 & 0 & 0 & 0 & 0 & 0 & 0 & 0 & 0 & 0 \\ 0 & 0 & 0 & 0 & 0 & 0 & 0 & 0 & 0 & 0 \\ 0 & 0 & 0 & 0 & F_{C2} & 0 & 0 & 0 & 0 & 0 \\ 0 & 0 & 0 & 0 & 0 & 0 & 0 & F_{C3} & 0 & 0 \\ 0 & 0 & 0 & 0 & 0 & F_{C1} & 0 & 0 & 0 & 0 \\ 0 & 0 & 0 & F^*_{C3} & 0 & 0 & 0 & 0 & 0 & 0 \\ 0 & 0 & 0 & 0 & 0 & 0 & F^*_{C2} & 0 & 0 & 0 \\ 0 & 0 & 0 & 0 & 0 & 0 & 0 & 0 & 0 & 0 \\ 0 & 0 & 0 & 0 & 0 & 0 & 0 & 0 & 0 & 0 \end{bmatrix}$$
(i)

$$\begin{bmatrix} F_L & 0 & 0 & 0 & 0 & 0 & 0 & 0 & 0 & 0 & 0 \\ 0 & 0 & 0 & 0 & 0 & 0 & 0 & 0 & 0 & 0 & 0 \\ 0 & 0 & 0 & 0 & 0 & 0 & 0 & 0 & 0 & 0 & 0 \\ 0 & 0 & 0 & 0 & 0 & 0 & 0 & 0 & 0 & 0 & 0 \\ 0 & 0 & 0 & 0 & 0 & 0 & 0 & 0 & 0 & 0 & 0 \\ 0 & 0 & 0 & 0 & 0 & 0 & 0 & F_{C1} & 0 & 0 & 0 \\ 0 & 0 & 0 & 0 & F^*_{C1} & 0 & 0 & 0 & 0 & 0 & 0 \\ 0 & 0 & 0 & 0 & 0 & 0 & 0 & 0 & 0 & 0 & 0 \\ 0 & 0 & 0 & 0 & 0 & 0 & 0 & 0 & 0 & 0 & 0 \\ 0 & 0 & 0 & 0 & 0 & 0 & 0 & 0 & 0 & 0 & 0 \\ 0 & 0 & 0 & 0 & 0 & 0 & 0 & 0 & 0 & 0 & 0 \end{bmatrix}$$
(j)

the spectra of primary color components via the multiplexing matrix T:

$$\begin{bmatrix} F_L \\ F_{C1} \\ F_{C2} \end{bmatrix} = T \cdot \begin{bmatrix} R \\ G \\ B \end{bmatrix}, \tag{7}$$

where T can be written as

$$T = \begin{bmatrix} a_L^{(R)} & a_L^{(G)} & a_L^{(B)} \\ a_{C1}^{(R)} + i \cdot b_{C1}^{(R)} & a_{C1}^{(G)} + i \cdot b_{C1}^{(G)} & a_{C1}^{(B)} + i \cdot b_{C1}^{(B)} \\ a_{C2}^{(R)} + i \cdot b_{C2}^{(R)} & a_{C2}^{(G)} + i \cdot b_{C2}^{(G)} & a_{C2}^{(B)} + i \cdot b_{C2}^{(B)} \end{bmatrix}, \tag{8}$$

in which all a's and b's are real numbers. Note that the coefficients of R, G, and B channels for F_L must be real numbers because it is self-conjugate.

After plugging the expressions of the multiplex components in the frequency structure S_{CFA}, using the parameters in T, and applying the inverse symbolic DFT to S_{CFA}, we can have the expressions of primary CFA patterns written in the parameters in T, which are all *linear* functions. Therefore, if we could determine the optimal T, the optimal CFA pattern with the specified frequency structure can be obtained. Optimization based on T has several advantages. First, it is more natural as all our analysis is frequency based. Second, T has at most 15 (actually 10, as we will see in a moment) free parameters, making the search space relatively small. If we optimize in the spatial domain for the optimal primary CFA patterns directly, the number of free parameters will be $2n_xn_y$, which will be much larger when $n_xn_y > 8$.

The constraints on T now become apparent: the primary CFA patterns must all be real and nonnegative and their sum is an all-one matrix [14]. If the conjugate constraints in Section 3.1 are fulfilled when specifying the frequency

structure, it is guaranteed that the primary CFA patterns are all real. So we need not worry about this constraint. The nonnegativity would impose $3n_xn_y$ inequality constraints and the all-one summation would impose n_xn_y equalities on the parameters in T. However, the number of equality constraints can be greatly reduced if we consider them in the frequency domain. As that the sum of all primary CFA patterns being an all-one matrix is equivalent to that the sum of the first row of T is 1 and those of the remaining rows are all 0, it is more convenient to use the latter to replace the n_xn_y equality constraints on the parameters of T. Considering the real and the imaginary parts separately, there are 5 such equality constraints. So the number of free parameters in T is actually at most 10. It is possible that the 5 equality constraints are still not linearly independent, but it is harmless to keep all of them.

Now the search for the optimal T becomes the following constrained optimization problem:

$$\begin{cases} \text{Minimize} \ \| D \| \\ \text{Subject to: the (at most) 5 equality constraints and} \\ \qquad\qquad \text{the } 3n_xn_y \text{ inequality constraints,} \end{cases} \tag{9}$$

where $D = T^{-1}$ is the demosaicking matrix and the norm can be any matrix norm. Note that it is very tedious to write down all the inequality constraints manually as they involve the inverse symbolic DFT of the frequency structure, particularly when n_x or n_y is large. But this can be done on the computer via symbolic computing.

Although the feasible region of the parameters is convex (intersection of hyperspaces and half spaces), the objective function is not convex with respect to the parameters. Currently we have not developed an efficient method to find the globally optimal solution to problem (9), and only check the corners of the feasible region. However, we have found that the solution found in this way is already quite satisfactory.

Note that the primary colors that we have written in the previous sections and [14] are actually symbolic, i.e., 'RGB' can be real 'red', 'green', and 'blue', or real 'green', 'blue', and 'red', etc. So after obtaining an optimal CFA pattern w.r.t. the symbolic 'RGB', we can designate 'R', 'G', and 'B' as any permutation of real 'red', 'green', and 'blue'. Which pattern performs best is determined by the statistics of red, green, and blue colors in natural images.

5 A Design Example and New CFA Patterns

The steps of our CFA design methodology described in the previous two sections is summarized in Fig. 4. In the following, we give a detailed example of designing a 2×2 CFA pattern by using the proposed methodology. We also present several new CFA patterns designed using our method.

5.1 CFA pattern design of size 2×2

Our example follows the steps in Fig. 4.

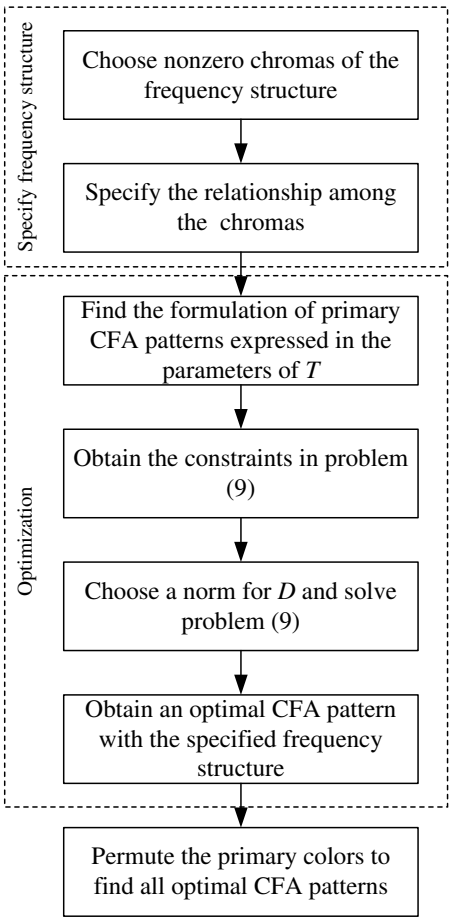

Figure 4: The flowchart of CFA pattern design.

Step 1. We choose the frequency structure of the 2×2 CFA pattern to be (Fig. 3(a)):

$$S = \begin{bmatrix} F_L & F_{C1} \\ 0 & F_{C2} \end{bmatrix}, \tag{10}$$

where we specify the chroma at $(0, 0.5)$ to be zero. Note that F_{C1} and F_{C2} are both self-conjugate. So their coefficients must all be real. Thus the multiplexing matrix is:

$$T = \begin{bmatrix} a_L^{(R)} & a_L^{(G)} & a_L^{(B)} \\ a_{C1}^{(R)} & a_{C1}^{(G)} & a_{C1}^{(B)} \\ a_{C2}^{(R)} & a_{C2}^{(G)} & a_{C2}^{(B)} \end{bmatrix}.$$

Step 2. As there are no redundant chromas, there is no relationship to prescribe between F_{C1} and F_{C2}.

Step 3. By applying inverse symbolic DFT to $S^{(\mathcal{C})}$, the primary CFA pat-

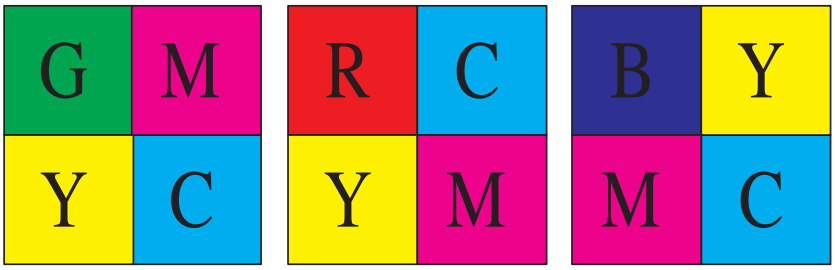

(a) (b) (c)

Figure 5: Designed CFA pattern of size 2×2 whose primary colors are (a) [R, G, B], (b) [G, R, B] and (c) [R, B, G].

terns are found to be ($\mathcal{C} = R, G, B$):

$$h_p^{(\mathcal{C})} = \begin{bmatrix} a_L^{(\mathcal{C})} + a_{C1}^{(\mathcal{C})} + a_{C2}^{(\mathcal{C})} & a_L^{(\mathcal{C})} - a_{C1}^{(\mathcal{C})} - a_{C2}^{(\mathcal{C})} \\ a_L^{(\mathcal{C})} + a_{C1}^{(\mathcal{C})} - a_{C2}^{(\mathcal{C})} & a_L^{(\mathcal{C})} - a_{C1}^{(\mathcal{C})} + a_{C2}^{(\mathcal{C})} \end{bmatrix}. \tag{11}$$

Step 4. The equality constraints are:

$$\begin{cases} a_L^{(R)} + a_L^{(G)} + a_L^{(B)} &= 1, \\ a_{C1}^{(R)} + a_{C1}^{(G)} + a_{C1}^{(B)} &= 0, \\ a_{C2}^{(R)} + a_{C2}^{(G)} + a_{C2}^{(B)} &= 0, \end{cases} \tag{12}$$

which are for making the sum of primary CFA patterns an all-one matrix. Note that now we only have 3 equality constraints because the zero sum constraints on the imaginary parts of the parameters in T are automatically fulfilled. And the inequality constraints are:

$$\begin{cases} a_L^{(\mathcal{C})} + a_{C1}^{(\mathcal{C})} + a_{C2}^{(\mathcal{C})} &\geq 0, \\ a_L^{(\mathcal{C})} - a_{C1}^{(\mathcal{C})} - a_{C2}^{(\mathcal{C})} &\geq 0, \\ a_L^{(\mathcal{C})} + a_{C1}^{(\mathcal{C})} - a_{C2}^{(\mathcal{C})} &\geq 0, \\ a_L^{(\mathcal{C})} - a_{C1}^{(\mathcal{C})} + a_{C2}^{(\mathcal{C})} &\geq 0, \end{cases} \quad \mathcal{C} = R, G, B, \tag{13}$$

which are for making the entries of the primary CFA patterns (11) nonnegative.

Step 5. Now we choose the 2-norm as the norm of D and solve the following optimization problem:

$$\begin{cases} \text{Minimize } \| D \|_2 \\ \text{Subject to: Eqs. (12) and (13).} \end{cases} \tag{14}$$

Step 6. After solving problem (14), we obtain a new CFA pattern

$$h_p = \begin{bmatrix} G & \frac{R+B}{2} \\ \frac{R+G}{2} & \frac{G+B}{2} \end{bmatrix}, \tag{15}$$

which is shown in Fig. 5(a). Its frequency structure is:

$$S = \frac{1}{4} \begin{bmatrix} R + 2G + B & G - B \\ 0 & -R + G \end{bmatrix}. \tag{16}$$

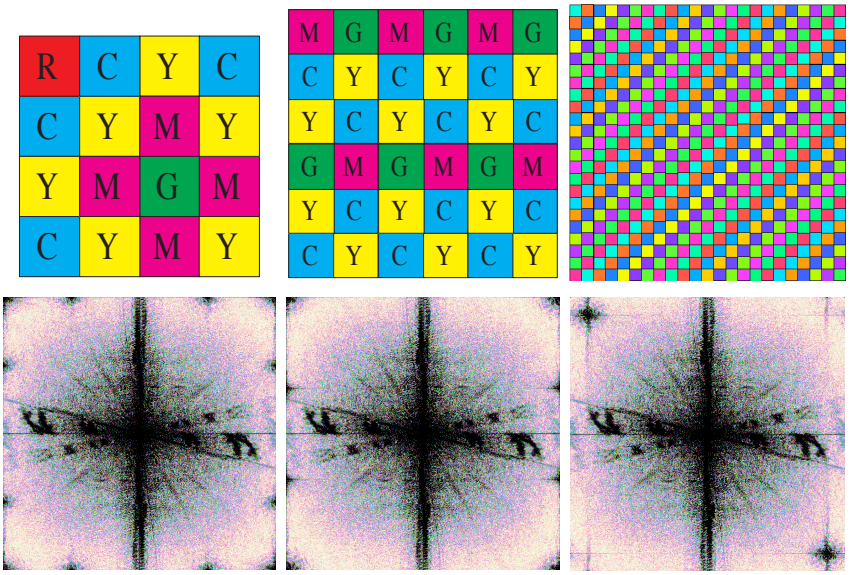

(a) (b) (c)

Figure 6: The proposed CFA patterns (a) CFA4a, (b) CFA6, (c) CFA23, and the spectra of images 'lighthouse' filtered with them.

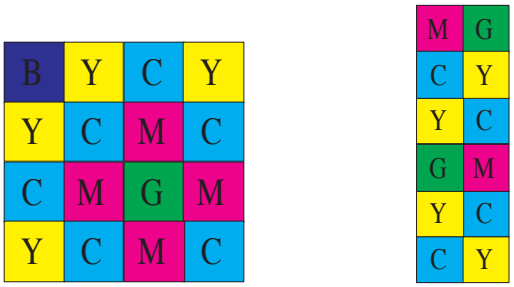

(a) (b)

Figure 7: (a) CFA4b, obtained by exchanging the red and blue color in CFA4a. (b) An equivalence of CFA6.

Step 7. Permuting R, G, and B in Eq. (15), we can totally have 6 optimal CFA patterns with the specified frequency structure (10), two of which are shown in Figs. 5(b)-(c), where the RGB corresponds to real 'green', 'red', and 'blue', and real 'red', 'blue', and 'green', respectively.

5.2 New patterns: CFA4a, CFA4b, CFA6 and CFA23

Using our design methodology, we have found several new CFA patterns of various sizes: CFA4a (4×4), CFA6 (6×6), and CFA23 (23×23). They are shown in Figs. 6 (a), (b), and (c), respectively.

The frequency structures of CFA4a and CFA6 are respectively:

$$S_{CFA4a} = \begin{bmatrix} F_L & 0 & 0 & 0 \\ 0 & 0 & F_{C2} & 0 \\ 0 & F_{C2} & F_{C1} & F_{C2} \\ 0 & 0 & F_{C2} & 0 \end{bmatrix}, \tag{17}$$

where

$$\begin{bmatrix} F_L \\ F_{C1} \\ F_{C2} \end{bmatrix} = \frac{1}{8} \begin{bmatrix} 3 & 3 & 2 \\ 1 & 1 & -2 \\ 1 & -1 & 0 \end{bmatrix} \cdot \begin{bmatrix} R \\ G \\ B \end{bmatrix}, \tag{18}$$

and

$$S_{CFA6} = \begin{bmatrix} F_L & 0 & 0 & 0 & 0 & 0 \\ 0 & 0 & 0 & F_{C2} & 0 & 0 \\ 0 & 0 & 0 & 0 & 0 & 0 \\ 0 & 0 & 0 & F_{C1} & 0 & 0 \\ 0 & 0 & 0 & 0 & 0 & 0 \\ 0 & 0 & 0 & F_{C2} & 0 & 0 \end{bmatrix}, \tag{19}$$

where

$$\begin{bmatrix} F_L \\ F_{C1} \\ F_{C2} \end{bmatrix} = \frac{1}{12} \begin{bmatrix} 3 & 6 & 3 \\ 3 & -2 & -1 \\ 0 & -2 & 2 \end{bmatrix} \cdot \begin{bmatrix} R \\ G \\ B \end{bmatrix}. \tag{20}$$

The nonzero multiplex components of CFA23 are respectively:

$0.332R + 0.334G + 0.334B$ at the baseband,
$(-0.166-0.023i)R+(0.103-0.132i)G+(0.063+0.155i)B$ at $(10/23, 10/23)$,
and
$(-0.166+0.023i)R+(0.103+0.132i)G+(0.063-0.155i)B$ at $(-10/23, -10/23)$.

The spectra of the image 'lighthouse' filtered with CFA4a, CFA6, and CFA23 are shown in the second row of Fig. 6, respectively.

If we exchange the primary colors R and B in CFA4a, we can obtain another new CFA, denoted as CFA4b (Fig. 7(a)). Its frequency structure is the same as that of CFA4a but the multiplexing matrix becomes

$$T_{CFA4b} = \frac{1}{8} \begin{bmatrix} 2 & 3 & 3 \\ -2 & 1 & 1 \\ 0 & -1 & 1 \end{bmatrix}. \tag{21}$$

Since the columns of CFA6 pattern have three periods, the CFA6 pattern is actually equivalent to a 6×2 pattern, as shown in Fig. 7(b).

6 Experiments

Now we test our new CFA patterns with the 24 widely-used Kodak color images [4, 8] and compare them with the Bayer pattern, and three CFAs proposed by Hirakawa and Wolfe [11], denoted as HWp1 (Fig. 1(k)), HWp2, and HWp3 (Fig. 1(l)).

As described previously, we apply the universal demosaicking method (Section 2) to the images sampled by the CFA patterns to be tested. For HWp1,

Table 2: CPSNR of demosaicking algorithms based on the Bayer CFA, three CFAs proposed in [11], and four our newly designed CFAs. As the performance of the Adaptive method for HWp1, HWp2, and CFA6 improves very little on its Naive counterpart, we do not list the corresponding CPSNRs due to limited space.

	Bayer				HWp1	HWp2	HWp3	CFA4a		CFA4b		CFA6	CFA23
Img.	Homo	POCS	Naive	Adapt	Naive	Naive	Direct	Naive	Adapt	Naive	Adapt	Naive	Direct
1	35.13	37.82	35.55	38.14	39.94	39.43	39.36	39.48	39.65	40.31	40.39	40.16	**40.82**
2	39.10	39.58	39.20	39.82	40.71	38.77	40.23	39.85	39.92	41.46	41.41	**41.57**	40.53
3	41.21	**41.66**	40.99	41.28	40.76	39.89	40.67	41.31	41.64	40.94	41.13	41.12	41.32
4	39.00	40.07	40.59	40.68	40.30	38.38	40.29	40.15	40.24	41.80	**41.88**	41.57	40.19
5	35.42	37.57	37.08	37.68	37.27	36.28	37.15	37.17	**37.82**	37.09	37.47	36.82	37.19
6	37.61	38.65	36.94	39.95	40.84	40.31	40.58	40.16	40.82	40.63	**41.06**	40.78	41.03
7	40.51	41.74	41.72	42.09	41.32	40.24	41.28	41.94	**42.16**	41.49	41.64	41.57	41.47
8	33.77	35.35	31.85	35.13	37.75	37.16	37.19	37.25	37.56	37.76	**37.97**	36.78	37.65
9	40.93	41.91	40.51	42.02	42.10	41.61	41.88	42.31	**42.48**	41.70	41.85	41.56	42.23
10	40.58	42.07	41.49	42.12	42.06	41.31	42.35	41.96	42.56	42.18	42.56	42.23	**42.66**
11	37.53	39.29	38.07	39.74	40.50	39.38	39.76	39.87	40.19	40.78	**41.01**	40.41	40.09
12	41.68	42.68	41.11	43.10	43.12	42.22	43.27	43.55	43.81	43.81	**43.94**	43.55	43.84
13	31.36	34.42	34.06	34.93	34.96	**35.48**	34.22	34.61	34.97	34.88	35.10	35.11	35.16
14	35.29	**35.91**	35.31	35.55	35.74	33.92	35.10	35.54	35.64	35.73	35.80	35.87	34.97
15	37.84	39.35	39.41	39.45	39.23	38.09	39.42	39.15	39.45	40.24	**40.44**	40.06	39.22
16	41.47	41.87	39.74	43.78	44.29	43.94	43.80	43.80	44.35	44.10	44.42	44.47	**44.48**
17	39.23	41.49	40.93	41.32	41.67	**41.70**	41.34	41.27	41.62	41.26	41.50	40.97	41.05
18	34.47	**37.24**	36.78	37.01	36.91	36.71	36.29	36.75	36.98	36.82	36.96	37.06	36.80
19	38.35	39.90	36.49	40.27	**41.73**	41.19	41.18	41.16	41.32	41.32	41.41	40.60	41.26
20	39.03	40.69	39.75	40.15	**41.48**	40.93	40.86	40.88	41.18	40.74	40.93	40.28	41.12
21	36.56	38.97	37.47	38.70	**40.27**	39.82	39.63	39.82	40.08	40.07	40.21	40.22	39.85
22	36.35	37.90	36.98	37.76	38.17	37.63	38.18	38.27	38.30	38.29	**38.31**	38.23	38.24
23	41.69	41.92	41.83	41.99	42.06	40.39	41.67	42.10	42.20	42.19	42.22	**42.28**	41.85
24	32.97	34.67	34.32	34.66	**35.44**	35.27	35.26	35.03	35.34	35.28	35.42	35.37	35.38
Avg.	37.80	39.28	38.26	39.47	39.94	39.17	39.62	39.72	40.01	40.04	**40.21**	39.94	39.93

HWp2, CFA4a, CFA4b, and CFA6, there may be identical or dependent chromas modulated at different frequency points. There are many methods to combine these copies for more accurate estimation of the chromas. One method is to naively average these copies.[1] The other method is the locally adaptive weighting method proposed in [4], which gives larger weights to the copies with less aliasing. The latter method respects the fact that these copies suffer different amount of aliasing. We shall call these two methods the *naive* and the *adaptive* method, respectively. For HWp3 and CFA23, there are only two chromas, which can only be estimated by direct band-pass filtering. Therefore, we denote these universal demosaicking algorithms as *HWp3-Direct* and *CFA23-Direct*, respectively.

For the Bayer CFA, CFA4a, and CFA4b, the Adaptive method outperforms the Naive method greatly, especially for the Bayer CFA (1.2 dB gain on average), which is not the case for HWp1, HWp2, and CFA6 (about 0.05 dB gain on average). We conjecture that the reason may lie in the combination characteristics of the Adaptive method. In general, the more difference several estimates have, the more gain we can obtain by combining the estimates. Thus, for the

[1] If two chromas, $S(p,q)$ and $S(r,s)$, are dependent, which means that there exists a scalar c such that $S(p,q) = c \cdot S(r,s)$ (Section 3.1), then we can average $S(p,q)/c$ and $S(r,s)$ for a better estimation of $S(r,s)$.

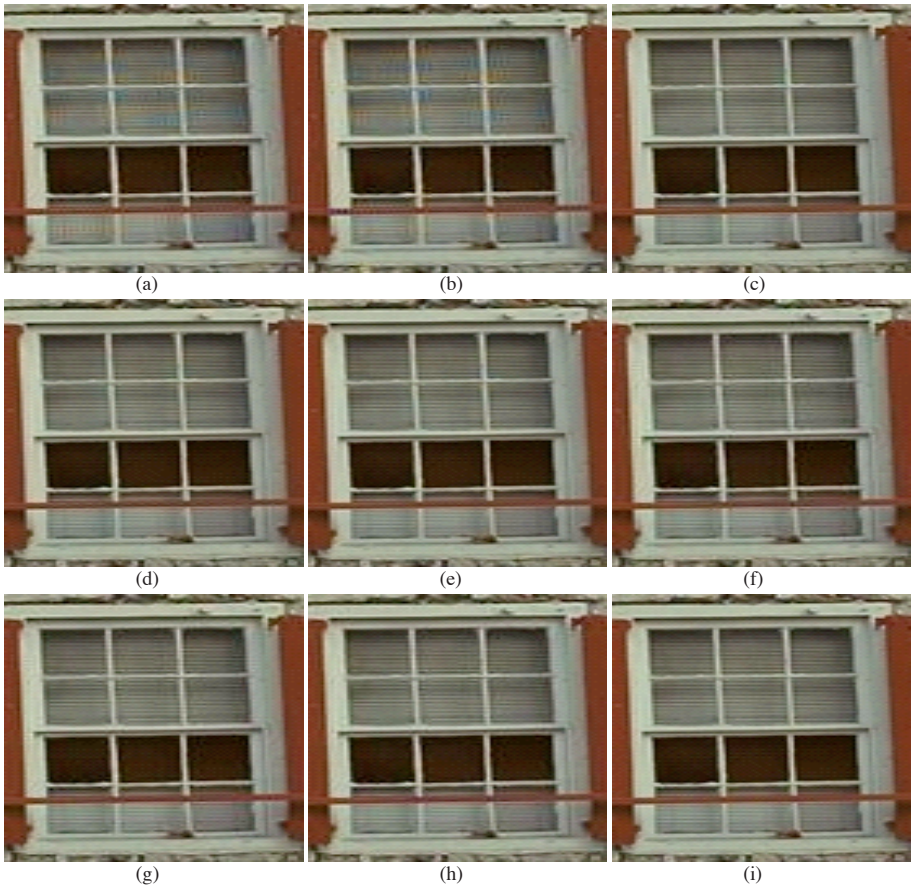

Figure 8: Parts of the demosaicked results of Image 1. (a) Bayer-POCS. (b) Bayer-Adapt. (c) HWp1-Naive. (d) HWp2-Naive. (e) HWp3-Direct. (f) CFA4a-Naive. (g) CFA4b-Adapt. (h) CFA6-Naive. (i) CFA23-Direct.

Bayer CFA, its two chromas ($(R-B)$ and $-(R-B)$) for combination lie on the horizontal and vertical axes and the noise suffered mainly from the luma is quite different, which leads to the great gain of the Adaptive method over the Naive one. Therefore, the gain of the Adaptive method is closely related to the frequency structure of a CFA. To save space, for the Adaptive method [4], we only show the results of the Bayer CFA, CFA4a, and CFA4b.

For better comparison, we also include two demosaicking algorithms for the Bayer CFA, the method of projection onto convex sets (*Bayer-POCS*) [7] and the homogeneity-directed one (*Bayer-Homo*) [10], which gave the best performance as compared in [8].

Table 2 gives the CPSNR (color-peak SNR, in dB) of each image and the average over 24 images. Clearly, the results with our new CFAs are much better than those with the Bayer CFA. Our new CFAs achieve the highest average CPSNR and the highest CPSNR for most of the images. Among the Bayer CFA-based algorithms, the Bayer-Adapt gives the best results. Though the adaptive

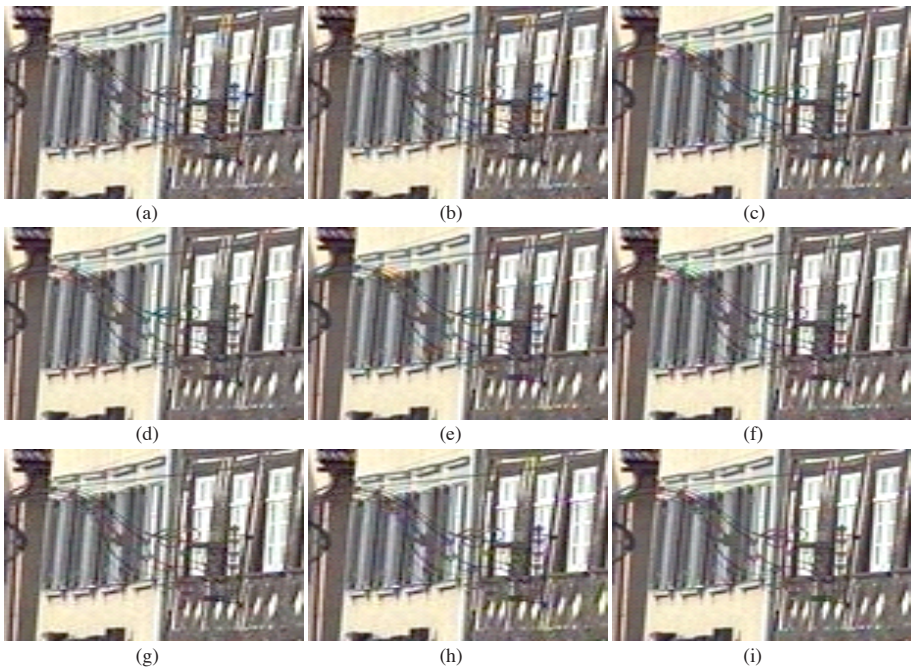

Figure 9: Parts of the demosaicked results of Image 8. (a) Bayer-POCS. (b) Bayer-Adapt. (c) HWp1-Naive. (d) HWp2-Naive. (e) HWp3-Direct. (f) CFA4a-Naive. (g) CFA4b-Adapt. (h) CFA6-Naive. (i) CFA23-Direct.

technique used in Bayer-Adapt greatly improves the performance with the Bayer CFA, our simple and non-adaptive CFA4a-Naive, CFA4b-Naive, CFA6-Naive, and CFA23-Direct algorithms still outperform Bayer-Adapt on average and on most of the 24 images. This demonstrates that using our new patterns, CFA4a, CFA4b, CFA6, and CFA23, the demosaicking quality can be improved a lot. The three patterns of [11], which simply aim to improve the arrangements of the multiplex components, only have relatively good results. HWp1, which is the best among them, is worse than the best (CFA4b) of our new CFA patterns and only has comparable performance with the other three of ours, in terms of average CPSNR. The other two patterns of [11], HWp2 and Hwp3, perform worse than all of our new CFA patterns.

Fig. 8, 9, and 10 provide the demosaicked images for the Images 1, 8, and 19. To save space, for CFA4a and CFA4b, we present only the results of CFA4a-Naive and CFA4b-Adapt, which have the worst and the best performance on average in terms of CPSNR, respectively, and for the Bayer pattern we present those of Bayer-POCS and Bayer-Adapt, which have better performance on average in terms of CPSNR. The figures show that for the window of Image 1 (Fig. 8) and the picket fence of Image 19 (Fig. 10), the output images of the Bayer CFA have obvious artifacts even with sophisticated demosaicking algorithms, while those of our new CFAs show very few artifacts, even with simple (the *Naive*) algorithms. As a matter of fact, this is an inherent problem of the Bayer CFA, since its spectrum has serious crosstalk along the horizontal and vertical

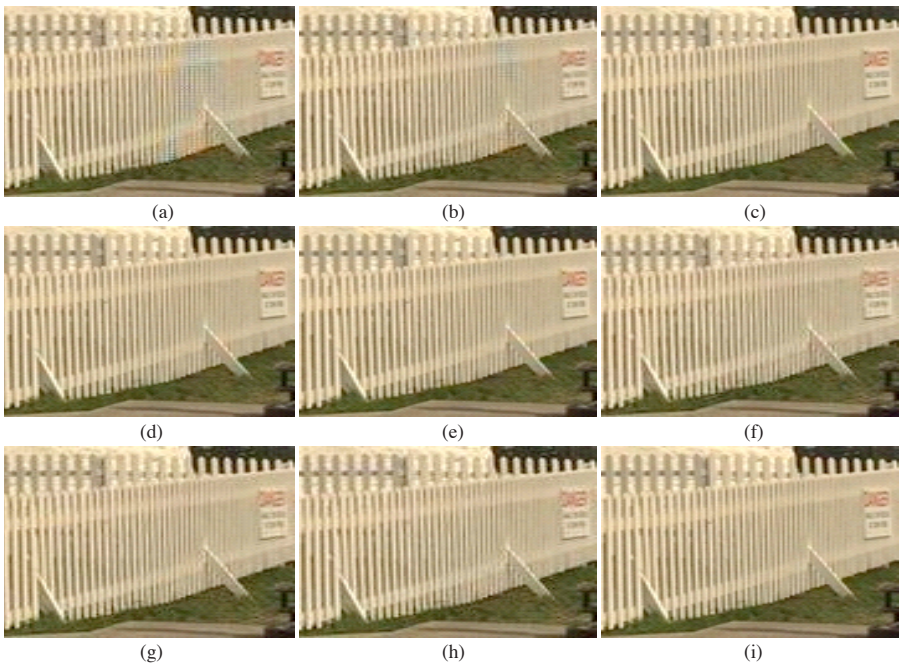

Figure 10: Parts of the demosaicked results of Image 19. (a) Bayer-POCS. (b) Bayer-Adapt. (c) HWp1-Naive. (d) HWp2-Naive. (e) HWp3-Direct. (f) CFA4a-Naive. (g) CFA4b-Adapt. (h) CFA6-Naive. (i) CFA23-Direct.

axes, which can be observed from its frequency structure (for details, see the CFA analysis in [14]). Thus for images whose spectra are relatively high along the horizontal and vertical axes, which is usually the case for natural images [14], the Bayer CFA is doomed to perform badly. For the wires of Image 8 (Fig. 9), CFA4b-Adapt outperforms others in terms of subjective quality. As the presence of wires corresponds to high energy in the area off the horizontal and vertical axes in the frequency space, severe aliasing may result for our new CFAs. However, by exploiting the correlations [4] among the nonzero chromas (e.g., 4 replica of $(R-G)/8$ for CFA4a, 4 replica of $(-G+B)/8$ for CFA4b, which contain different amount of aliasing), our new CFAs still perform well in terms of both CPSNR (Table 2) and subjective quality. The result images of HWp1, HWp2, and HWp3 have less obvious artifacts than those of Bayer, but still have some. For example, the color Moiré artifact on the fence support of the picket fence of Image 19 (Figs. 10(c)-(e)) is visible.

For the Bayer, HWp1, HWp2, and HWp3 CFAs, we have also tested their alternative CFAs obtained by permuting the colors R, G and B, and compared them with our CFAs in terms of average CPSNR. For the Bayer CFA, if we exchange R and G, the average CPSNR is the highest (39.71 dB) for demosaicking with the Adaptive method. For HWp1, its alternatives cannot lead to better results. As a matter of fact, the average CPSNR is 39.17 dB if G and B exchange, and 38.88 dB if R and G exchange. For HWp2, the average CPSNR is the highest when G and B exchange (39.53 dB) but is still lower than that

of the Bayer CFA exchanging R and G and those of all our CFAs. For HWp3, we cannot obtain better results by permuting the color. Thus HWp1 and its alternatives are all worse than CFA4b, and are worse than or comparable to our other CFAs. The results of Bayer, HWp2, and HWp3 CFAs and their alternatives are all worse than those of our proposed CFAs. This implies that the proposed methodology can find better than ever or even the best CFAs.

7 Conclusions and Future Work

Based on the frequency domain representation of CFAs, a CFA design methodology is proposed in this paper. It aims at minimizing the demosaicking error by better arranging multiplex components in the frequency structure and finding the optimal multiplexing matrix. Our experiments show that using our new CFA patterns, the simple universal demosaicking algorithm can achieve excellent demosaicking quality.

The performance of the universal demosaicking algorithm can be further improved if better methods for combining the duplicated chromas could be found. And a fast method to find the globally optimal solution to (9) is also desirable. These are two of our future work. And actually the different chromas should not be limited to two (e.g., we can specify conjugate relationship among the chromas to have frequency structures like that of Kodak in Table 1 of [14]) such that the multiplexing matrix is of size $K \times 3$, where $K > 3$. In this case, how to accurately estimate these chromas and the spectra of primary color components is also worth exploring.

References

[1] J. Adams, K. Parulski, and K. Spaulding. Color processing in digital cameras. IEEE Micro, vol. 18, no. 6, pp. 20-31, 1998.

[2] D. Alleysson, S. Susstrunk, and J. Herault. Linear demosaicing inspired by the human visual system. IEEE Trans. Image Process., 14(4):439-449, 2005.

[3] B.E. Bayer. Color imaging array. U.S. Patent 3 971 065, 1976.

[4] E. Dubois. Frequency-domain methods for demosaicking of Bayer-sampled color images. IEEE Signal Process. Lett., 12:847-850, 2005.

[5] FillFactory. Technology image sensor: the color filter array.

[6] E.B. Gindele and A.C. Gallagher. Sparsely sampled image sensing device with color and luminance photosites. U.S. Patent 6 476 865 B1, 2002.

[7] B.K. Gunturk, Y. Altunbasak, and R.M. Mersereau. Color plane interpolation using alternating projections. IEEE Trans. Image Processing, vol. 11, no. 9, pp. 997-1013, Sept. 2002.

[8] B.K. Gunturk, J. Glotzbach, Y. Altunbask, R.W. Schafer, and R.M. Mersereau. Demosaicing: Color filter array interpolation. IEEE Signal Process. Mag., 22(1):44-54, 2005.

[9] J.F. Hamilton, J.E. Adams, and D.M. Orlicki. Particular pattern of pixels for a color filter array which is used to derive luminanance and chrominance values. U.S. Patent 6 330 029 B1, Dec. 2001.

[10] K. Hirakawa and T. W. Parks. Adaptive homogeneity-directed demosaicing algorithm. IEEE Trans. Image Process., 14(3):360-369, 2005.

[11] K. Hirakawa and P.J. Wolfe. Spatio-Spectral Color Filter Array Design for Enhanced Image Fidelity. Proc. IEEE Int. Conf. Image Processing, 2007.

[12] ——. Fourier Domain Display Color Filter Array Design. Proc. IEEE Int. Conf. Image Processing, 2007.

[13] Kodak Press Release. [online]. June 2007. Available at: www.dpreview.com/news/0706/ 07061401kodakhighsens.asp.

[14] Y. Li, P. Hao, and Z. Lin. Color filter arrays: representation and analysis. Technical Report, Department of Computer science, Queen Mary, University of London, 2008.

[15] R. Lukac and K. N. Plataniotis. Color filter arrays: Design and performance analysis. IEEE Trans. Consum. Electron., 51(4):1260-1267, 2005.

[16] M. Parmar and S. J. Reeves. A perceptually based design methodology for color filter arrays. Proc. Int. Conf. Acoustics, Speech, and Signal Proc., 473-476, 2004.

[17] M. Parmar and S. J. Reeves. Selection of optimal spectral sensitivity functions for color filter arrays. Proc. IEEE Int. Conf. Image Processing, 2006, pp. 1005-1008.

[18] Sony Press Release. [Online]. 2003. Available at: http://www.sony.net/SonyInfo/News/Press/200307/03-029E/.

[19] M. Vrhel, E. Saber, and H.J. Trussell. Color image generation and display technologies. IEEE Signal Process. Mag., 22(1):23-33, Jan. 2005.

[20] T. Yamagami, T. Sasaki, and A. Suga. Image signal processing apparatus having a color filter with offset luminance filter elements. U.S. Patent 5323233, June 1994.

[21] S. Yamanaka. Solid state color camera. U.S. Patent 4 054 906, 1977.

[22] W. Zhu, K. Parker, and M.A. Kriss. Color filter arrays based on mutually exclusive blue noise patterns. J. Vis. Commun. Image Represent., vol. 10, pp. 245-247, 1999.